



## Low- and high-frequency fatigue of bulk metallic glasses

Yu. Petrusenko<sup>a,\*</sup>, A. Bakai<sup>a</sup>, I. Neklyudov<sup>a</sup>, S. Bakai<sup>a</sup>, V. Borysenko<sup>a</sup>,  
G. Wang<sup>b</sup>, P.K. Liaw<sup>b</sup>, L. Huang<sup>b,c</sup>, T. Zhang<sup>c</sup>

<sup>a</sup> National Science Center, Kharkov Institute of Physics & Technology, Kharkov 61108, Ukraine

<sup>b</sup> Department of Materials Science and Engineering, The University of Tennessee, Knoxville, TN 37996, USA

<sup>c</sup> Department of Materials Science and Engineering, Beijing University of Aeronautics and Astronautics, Beijing 100191, China

### ARTICLE INFO

#### Article history:

Received 14 August 2010

Received in revised form 21 January 2011

Accepted 29 January 2011

Available online 5 February 2011

#### Keywords:

Metallic glasses

Clusters

Point defects

Ultrasonics

### ABSTRACT

The 2.5 MeV electron-irradiation and resistance-recovery experiments were performed. It was found that the majority of atoms of a  $(Zr_{0.55}Al_{0.10}Ni_{0.05}Cu_{0.30})_{99}Y_1$  bulk metallic glass (BMG) possess a locally preferred order, and vacancies are stable point defects. Low- and high-frequency compression–compression fatigue experiments show that the fatigue-endurance limit and mode of the fatigue fracture of this BMG essentially depend on the cycling frequency. At the low-frequency cycling (10 Hz), the catastrophic crack is initiated mainly due to the shear-of-steps formation, and the fatigue-endurance limit is  $\sim 0.44 \sigma_{FS}$  ( $\sigma_{FS}$  is the fracture stress). At the high-frequency cycling (20 kHz), the catastrophic crack forms due to the propagation and mergence of nano-cracks initiated from slip layers at intercluster boundaries. The fatigue-endurance limit in this case is a random quantity with a mean value of  $\sim 0.04 \sigma_{FS}$ .

© 2011 Elsevier B.V. All rights reserved.

### 1. Introduction

Non-direct manifestations of the point and extended defects in the physical properties of metallic glasses are still an important tool of their structure features research. As it was shown in Ref. [1], stability and thermally activated mobility of point defects take place in polyclusters. Following the 2.5 MeV electron irradiation of bulk metallic glasses (BMGs) and resistance-recovery experiments [2,3], we have shown that the stable vacancies exist, at least within the investigated glasses, and that their diffusion mobility is thermally activated. The low-frequency (10 Hz) compression–compression fatigue experiments [4] reveal the importance of the large-scale shear-band formation in affecting the initiation and propagation behavior of the catastrophic crack. With that, the fatigue-endurance limit is comparatively high ( $\sim 0.44 \sigma_{FS}$ , where  $\sigma_{FS}$  is the fracture stress). In other words, the low-frequency cycling stress considerably facilitates the BMG fracture but do not allow to obtain more rich information about the structure features of BMGs than that obtained from their fracture at monotonically increasing compression.

In high-frequency fatigue (HFF) experiments using ultrasonic vibrations (20 kHz), the cycling stresses of small amplitudes can form small-scale inner slip layers, within the weak intercluster boundaries revealed by means of the field-emission microscopy

[5]. One can assume that the viscous dissipation of the mechanical energy and irreversible inelastic structure changes in the slip layers can initiate their propagation and initiation of inner nano-cracks. The propagation and mergence of the inner cracks can lead to the BMG fracture. Results of our experiments indicate that this scenario of the HFF fracture really takes place at rather low mean stresses and even lower amplitudes of cycling stresses.

### 2. Experimental

The method of the low-temperature electron irradiation of BMG samples with their subsequent isochronal annealing and electrical-resistance measurements was used in our experiments. Irradiation with 2.5 MeV electrons at  $\sim 80$  K was carried out at the ELIAS electrostatic accelerator of the National Science Center – Kharkov Institute of Physics and Technology. Irradiation, annealing, and resistance-measurement techniques are described in details [2].

A computer-controlled Material Test System (MTS) servohydraulic testing machine was employed for low-frequency fatigue (LFF) experiments. The machine was aligned prior to use, as required. Samples were tested at various stress ranges with an  $R$  ratio ( $R = \sigma_{min}/\sigma_{max}$ , where  $\sigma_{min}$  and  $\sigma_{max}$  are the applied minimum and maximum stresses, respectively) of 0.1 under a load-control mode, using a sinusoidal waveform at a frequency of 10 Hz. Upon failures or  $10^7$  cycles, samples were removed and stored for later examinations by a scanning-electron microscope (SEM) to identify fatigue-crack initiation and growth mechanisms. The fracture surfaces of selected specimens were examined, using a Leo 1526 SEM machine with the energy-dispersive spectroscopy to provide fatigue and fracture mechanisms.

The HFF experiments and pre-treatment of the specimens were done using the special test facility [6]. The specimens were clamped to the lowest cross-section of the ultrasonic concentrator. The specimen stress was 50 MPa. Thereafter, the 20 kHz vibrations were turned on. The amplitude of ultrasonic vibrations was from  $6 \mu m$  up to  $14 \mu m$ . The fractography of the fractured samples after fatigue testing was done on the Leica Z6APO microscope and on an SEM to study fatigue and fracture mechanisms.

\* Corresponding author. Tel.: +38 057 335 44 44; fax: +38 057 335 44 44.

E-mail address: [petrusenko@kipt.kharkov.ua](mailto:petrusenko@kipt.kharkov.ua) (Yu. Petrusenko).

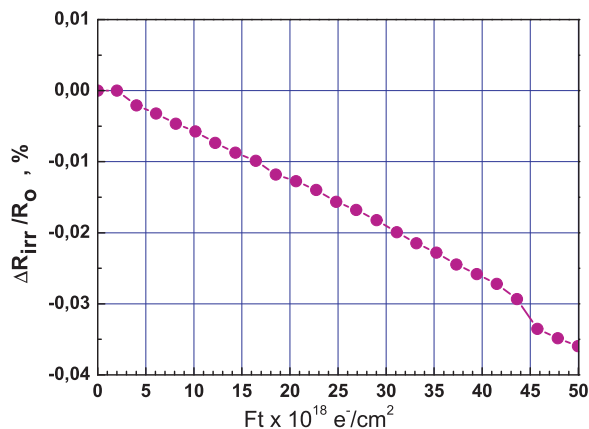


Fig. 1. Dose dependence of the relative electrical resistance for the  $(\text{Zr}_{0.55}\text{Al}_{0.10}\text{Ni}_{0.05}\text{Cu}_{0.30})_{99}\text{Y}_1$  BMG irradiated with 2.5 MeV electrons at  $\sim 80$  K.

### 3. Results

#### 3.1. Accumulation and recovery kinetics of radiation damages in $(\text{Zr}_{0.55}\text{Al}_{0.10}\text{Ni}_{0.05}\text{Cu}_{0.30})_{99}\text{Y}_1$

The dose dependence of the electrical resistance of the  $(\text{Zr}_{0.55}\text{Al}_{0.10}\text{Ni}_{0.05}\text{Cu}_{0.30})_{99}\text{Y}_1$  BMG sample irradiated with 2.5 MeV electrons at  $\sim 80$  K is presented in Fig. 1. The linear dependence of  $\Delta R_{\text{irr}}/R_0$  on electron fluence is a manifestation of storage of the irradiation effects without considerable interactions of the stored damages. Here  $\Delta R_{\text{irr}} = R_{\text{irr}} - R_0$ , where  $R_0$  and  $R_{\text{irr}}$  are electrical resistances before and after the irradiation with the maximum fluence, respectively. One can see a negative slope of the dose-dependence line of irradiated samples. As it was declared for other BMG composites [2,3], this feature can be explained as a result of the irradiation-induced atomic replacements, leading to short-range ordering of the alloy. In the frame of the polycluster-structure model of metallic glasses [7,8], the ordering process enhanced by the irradiation can take place in both the cluster body and intercluster boundaries. This process does not need a long-range diffusion and probably is an intrinsic property for most of the Zr-based BMGs.

Derivatives of isochronous recovery curves of radiation-induced resistance changes of  $(\text{Zr}_{0.55}\text{Al}_{0.10}\text{Ni}_{0.05}\text{Cu}_{0.30})_{99}\text{Y}_1$  (present work) and  $\text{Zr}_{52.5}\text{Ti}_5\text{Cu}_{17.9}\text{Ni}_{14.6}\text{Al}_{10}$ , and  $\text{Zr}_{46.8}\text{Ti}_{8.2}\text{Cu}_{7.5}\text{Ni}_{10}\text{Be}_{27.5}$  [2,3] BMGs are shown in Fig. 2.

Along with that, atomic displacements, i.e., stable Frenkel pairs (interstitial + vacancy), are generated by high energy electron beam in BMG. These point defects are unstable in the dense random packing of spheres (DRPS) but they are stable in the cluster body [1]. Therefore, no annealing stages of irradiated DRPS can exist. The situation is different in polyclusters. The cluster boundaries are sinks of the point defects. The activation energy of the interstitial diffusion is, as in crystals, much less than the activation energy of vacancies. Therefore, the annealing stages of interstitials are at much lower temperatures those of vacancies. In crystalline metals and alloys the interstitial annealing stages usually are in the temperature range below 120 K (see, e.g., [9]). Therefore, we believe that this two revealed annealing stages for each BMG composition are connected with the activation of mobility of the vacancies and vacancy-alloying addition complexes.

It should be noted that for all the studied BMGs, the temperature peaks and the estimated effective activation energies of recovery stages are observed to be close to each other. Thus, the temperature peak of the “high-temperature” stage at 225 K and the estimated effective activation energy of  $\sim 0.7$  eV coincide for all the investigated compositions. An effective activation energy of  $\sim 0.4$  eV and peak temperature of

125 K are almost identical for  $(\text{Zr}_{0.55}\text{Al}_{0.10}\text{Ni}_{0.05}\text{Cu}_{0.30})_{99}\text{Y}_1$  and  $\text{Zr}_{52.5}\text{Ti}_5\text{Cu}_{17.9}\text{Ni}_{14.6}\text{Al}_{10}$  BMGs, and only shifted to 150 K, with a corresponding increase of the effective activation energy up to 0.46 eV for the  $\text{Zr}_{46.8}\text{Ti}_{8.2}\text{Cu}_{7.5}\text{Ni}_{10}\text{Be}_{27.5}$  BMG. These data indicate that the observed recovery stages after low-temperature electron irradiation in the Zr-based BMGs are stipulated by migration or reorientation of identical or similar configurations of mainly vacancy-type point defects. To identify the actual configurations of radiation defects, it is necessary to perform similar experiments on simple, preferably two-component BMG compositions, as well as to carry out simulation processes of primary damage and annealing of the BMGs.

#### 3.2. Low- and high-frequency compression–compression fatigue and fracture

The LFF experiments were performed at the cycle frequency of 10 Hz,  $\sigma_{\text{max}} = 0.8, 0.9, 1.0,$  and 1.1 GPa, and the ratio,  $R = 0.1$ . The deformation rate was  $\langle \dot{\epsilon} \rangle \sim 0.5/\text{s}$ . The compression–compression fatigue results for the  $(\text{Zr}_{0.55}\text{Al}_{0.10}\text{Ni}_{0.05}\text{Cu}_{0.30})_{99}\text{Y}_1$  samples shows that the fatigue–endurance limit ( $\sigma_L$ ), based on the applied stress range, subjected to compression–compression loading is 0.8 GPa. Above the endurance limit, the fatigue lifetime generally decreases with increasing the stress level. The cyclic-compression fracture surface displays a morphology nearly identical to the monotonic-compression fracture surface. Most of the fracture surface is covered by vein-like patterns. These vein-like patterns formed due to the significant temperature increase when the sample failed. It was found that, as a rule, the catastrophic crack propagates from the surface [4,10]. The morphology of the low-frequency fatigued sample is seen from the SEM fractograph shown in Fig. 3a. Here the regions of the brittle cracking and ductile fracture are clearly seen. The vein pattern and frozen droplets are observed in the regions of the ductile fracture. The catastrophic crack is propagating at angle  $\approx 45^\circ$  to the external stress. At  $\sigma_{\text{max}} = \sigma_L$ , the number of cycles to fracture ( $N_f$ ) is greater than  $10^7$ . It occurs that  $N_f \sim 10^5$  at  $\sigma_{\text{max}} = 1$  GPa. The ratio of the fatigue–endurance limit to the fracture stress at monotonic compression,  $\sigma_{\text{FS}} = 1.8$  GPa, is 0.44. The obtained results are very similar to those of the LFF with a  $\text{Zr}_{50}\text{Al}_{10}\text{Cu}_{37}\text{Pd}_3$  BMG [4]. Therefore, we refer readers to Ref. [4] for detailed discussions of the low-frequency fatigue–fracture mode.

The HFF experiments were performed at the cycle frequency of 20 kHz, constant compression,  $\bar{\sigma} = 0.15$  GPa, and amplitudes of the vibrations,  $A = 6\text{--}14 \mu\text{m}$  or  $A/l_0 = \tilde{\epsilon} = (1.5\text{--}3.5) \times 10^{-3}$  ( $l_0$  is the initial length of the specimen). The ratio,  $\sigma_{\text{max}}/\sigma_{\text{FS}}$ , is less than 0.15. Thus, the experiments were performed in the region of elastic deformation but the rate of the cyclic deformation is high,  $\langle \dot{\epsilon} \rangle = 100\text{--}150/\text{s}$ . The high-frequency compression–compression fatigue–endurance limit is a random, very scattered quantity with a mean value of  $\sim 0.04 \sigma_{\text{FS}}$ . Some specimens were not fractured at  $\tilde{\epsilon} = 2.5 \times 10^{-3}$  and  $N = 6 \times 10^6$ , while others were fractured at  $\tilde{\epsilon} = 2 \times 10^{-3}$  and  $N = 5 \times 10^5$ . Even at  $\tilde{\epsilon} = 1.5 \times 10^{-3}$  after  $4 \times 10^6$  cycles, a noticeable decrease of  $\sigma_{\text{FS}}$  and Young’s modulus was observed.

The mode of the high-frequency compression–compression fatigue fracture is completely different from that at low-frequency cycling and large  $\sigma_{\text{max}}/\sigma_{\text{FS}}$  ratios, as it is seen in Fig. 3b, where the optical metallography of the fractured specimen and SEM fractography of a typical region of the fracture surface are shown. It is seen that the specimen fracture is caused by initiation, propagation, and mergence of multiple cracks in the specimen body. It has to be stressed that the resulting catastrophic crack has no specific orientations. It looks like a mergence of initially isolated inner nano-cracks into a percolating catastrophic crack. Nearly 20% of the fracture surface is covered by crystallites of sizes, 10–100 nm. Due to the presence of the crystallites, narrow lines appear in the

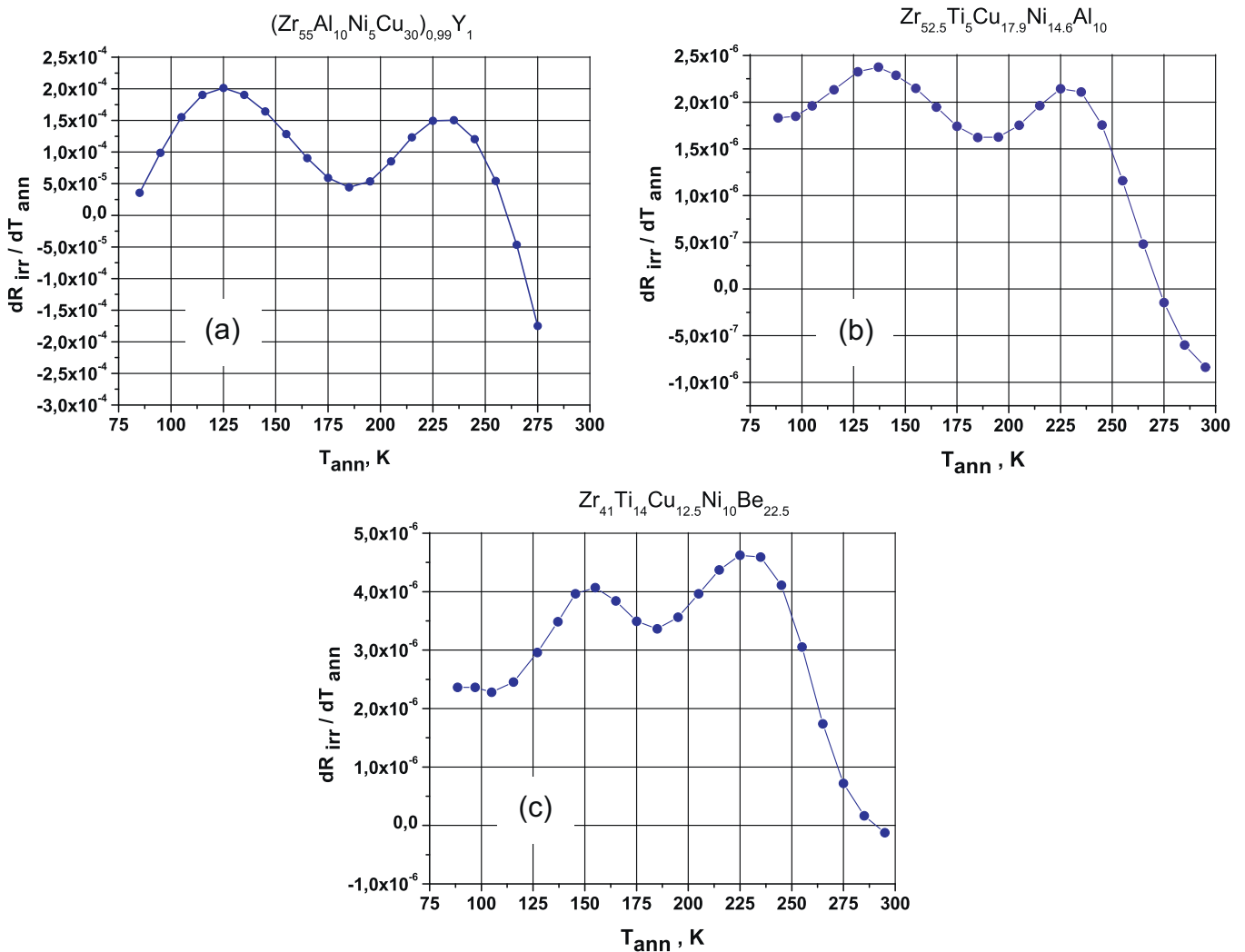


**Fig. 2.** Recovery spectrums of the irradiation-induced electrical resistance,  $R_{irr}$ , (derivatives,  $dR_{irr}/dT_{ann}$ , on the annealing temperature,  $T_{ann}$ ) for  $(Zr_{0.55}Al_{0.10}Ni_{0.05}Cu_{0.30})_{99}Y_1$  (a),  $Zr_{52.5}Ti_5Cu_{17.9}Ni_{14.6}Al_{10}$  (b), and  $Zr_{46.8}Ti_{8.2}Cu_{7.5}Ni_{10}Be_{27.5}$  (c), irradiated with 2.5 MeV electrons at  $\sim 80$  K.

X-ray diffraction on the fractured specimen. The positions of the lines show that the crystallites possess mainly a ZrAl lattice. Since for the partial crystallization of the glass, a diffusion mobility of atoms is needed, we can conclude that the local heating of the slip layers and crack surfaces due to the inner friction under the ultrasonic vibrations is considerable to provide the mobility of at least comparatively small Ni and Cu atoms. The mean specimen temperature was less than the glass-transition temperature. Otherwise, a homogeneous plastic deformation (a diffusion-viscous flow) could take place.

#### 4. Discussion

Since the LFF does not show any exceptional features, as compared to those observed in experiments with BMGs of different compositions [4, 10], we briefly discuss the peculiarities of the high-frequency investigations. As was noted, the mean deformation rate in HFF is large,  $\sim 10^2/s$ . Therefore, even at small amplitudes of the cycling deformation, the internal friction due to the anelastic deformation plays a significant role because the energy dissipation rate is  $\dot{E}_{fr} \sim \eta(\dot{\epsilon})^2 v_{fr}$  ( $\eta$  is the viscosity;  $v_{fr}$  is the volume of the regions where the anelastic deformation takes place). To specify the coefficients,  $\eta$  and  $v_{fr}$ , we have to note that metallic glasses, as they were revealed by means of the field-emission microscopy [5, 11], pos-

sess the polycluster structure [7, 8] with cluster sizes of  $\sim 10$  nm. The intercluster boundaries have a width less than 1 nm [5]. Thus, the fraction of atoms belonging to the boundaries is  $\sim 10^{-1}$  (compared with conclusions made in Ref. [12]). The maximal shear stress is in the boundary section oriented at the angle of  $\approx 45^\circ$  to the external stress. Let us denote this value as  $\sigma_m = \sigma(\pi/4)$ . Then the shear stress on the boundary section oriented at the angle  $\pi/4 + \theta$  is  $\sigma(\pi/4 + \theta) = \sigma_m \cos \theta \geq 0.995 \sigma_m$  at  $\theta < 0.1$ . Thus, on average, the fraction of such boundary sections can be estimated as  $\sim 10^{-1}$ . We have to take into account that the length of the slip layer,  $\lambda$ , determines the concentration of the stress in the mouth of the layer,  $\sigma_{mouth} \sim (\sigma_{shear}) (\lambda/a)^{1/2}$ ,  $a$  is the atom size,  $\sigma_{shear}$  is the shear stress in the layer. Thus, just comparatively long slip layers can propagate and initiate nano-cracks. Taking the fraction of long slip layers to be of the order of  $10^{-1}$ , we have a crude estimation of the dissipation-energy rate,  $\dot{E}_{fr} \sim 10^{-3} \eta(\dot{\epsilon})^2 V$ ,  $V$  is the specimen volume. The shear viscosity at low temperatures is  $\eta \sim \sigma/(\dot{\epsilon})$  because in the slip layer, the external shear stress,  $\sigma$ , is larger or equal to the boundary yield stress.

Proceeding from the made remarks and estimations, we can interpret the obtained results of the HFF as follows. In spite of the fact that the amplitudes of the cycling compression strains are comparatively small,  $\tilde{\epsilon} \sim 10^{-3}$ , they are able to produce significant anelastic and then inelastic deformations, propagation of the slip

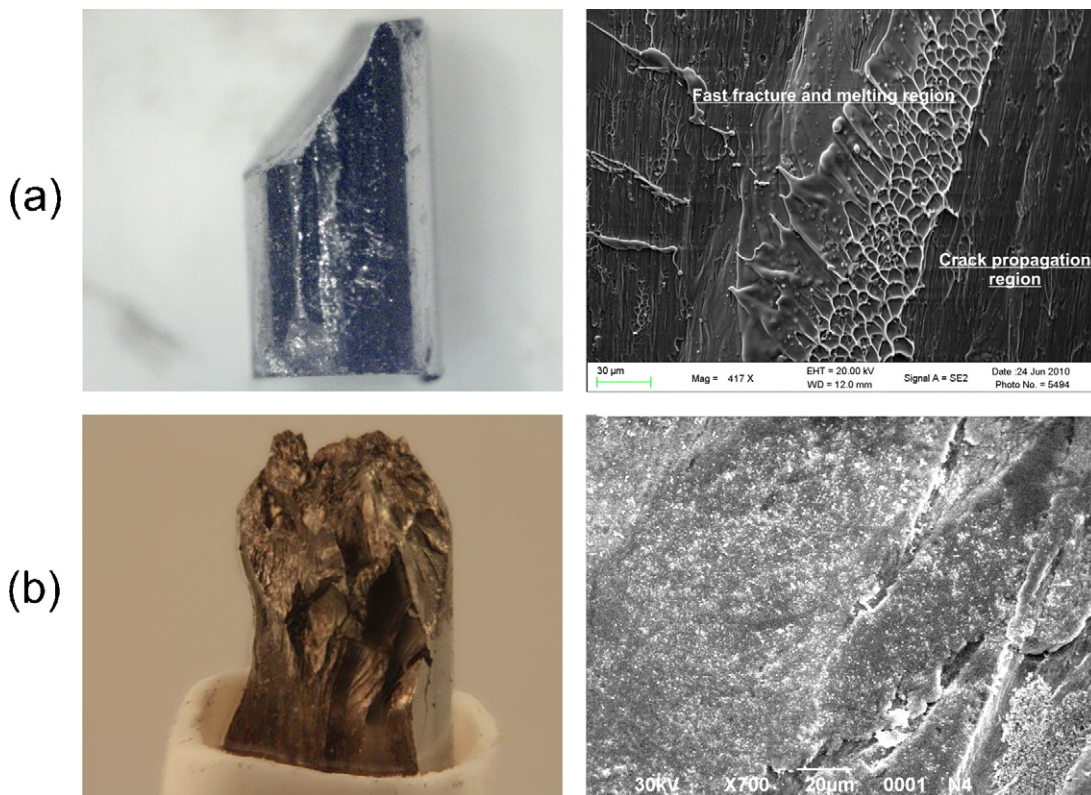


**Fig. 3.** (a) Optical microscopy and SEM of a fragment of the fracture surface for low-frequency fatigue; (b) Optical microscopy and SEM of the fracture surface of the high-frequency fatigue-fractured specimen. Crystallites (light spots) cover ~20% of the crack surface. Treatment for 25 min. ( $N = 30,000,000$ ) at an amplitude,  $A = 14$  microns.

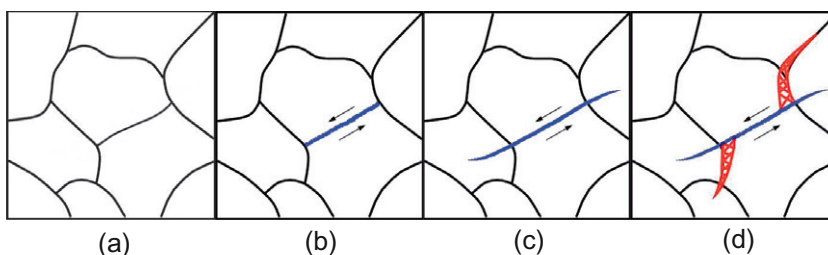


**Fig. 4.** Scheme of nano-cracks initiation from the slip layers in the polycluster boundaries: (a) an area of polycluster before compression, intercluster boundaries are shown; (b) a slip layer formed under compression stresses, arrows show directions of the mean shear stress; (c) a slip layer propagates due to the action of the cycling stress; and (d) nano-cracks along the intercluster boundaries are initiated.

layers, and initiation and propagation of the nano-cracks for two reasons.

First, the probability of the “long” slip-layer formation in the properly oriented boundaries is comparatively large,  $\sim 10^{-3}$  of all atoms are involved in the anelastic and inelastic deformations, which lead to the nano-crack formation and propagation. The observed large uncertainty of the fatigue-endurance limit is caused by uncontrolled nano-scale structure heterogeneities and extended defects of the tested specimens.

Second, due to the internal friction caused by anelastic and inelastic processes, a considerable amount of the deformation energy is transforming into heat and increases the temperature of the specimen. The heat enhances the diffusional activity and induces the observed crystallization. The low thermal conductivity of BMGs ( $\sim 4-7 \times 10^{-3}$  W/cm K) [13] provides an essential increase of the specimen temperature in spite of its contacts with massive details of the test device. The temperature increase facilitates the thermal activation of the slip layers and nano-crack propagation and mergence. It has to be noted that at LFF, the heating effect becomes essential just at the last, fast fracture stage.

In Fig. 4, different initial stages of the non-elastic deformation are schematically shown for BMG polyclusters. One can see that the slip layer initiated by external cycling-compression stresses at the intercluster boundary is propagating and initiating nano-cracks. Propagation and mergence of the nano-cracks in the specimen body lead to the fracture.

## 5. Conclusions

- The annealing stages of the irradiated specimens reveal the existence of two annealing stages above 100 K. They are attributed to the stable vacancies and vacancy complexes in BMGs. The vacancy mobility is a thermally activated process as it has to be in polyclusters.
- Compression-compression LFF and HFF experiments show that the fatigue-endurance limit and the fracture mode essentially depend on the frequency.
- At LFF, the catastrophic crack angle is nearly  $\pi/4$ , and the fracture surface is consisting of the crack-initiation, crack-propagation, fast fracture, and melting regions.

- At HFF, multiple inner nano-cracks initiation, propagation, and merge take place at rather small strain amplitudes,  $\tilde{\epsilon} \sim 10^{-3}$ . On average the catastrophic crack-propagation direction forms the considerably less than  $\pi/4$  angle with the stress direction. The fatigue-endurance limit is a random quantity with large dispersion. The release of the comparatively large deformation energy due to the friction in the slip layers and cracks produces local heat, resulting in the acceleration of the crack propagation, diffusion enhancement, and growth of crystallites. The fraction of the fracture surface covered by the crystalline precipitates reaches  $\sim 20\%$ .
- One can conclude that ultrasonic vibrations induce irreversible changes of the BMG structure even at small amplitudes.

### Acknowledgement

Yu. Petrusenko, A. Bakai, I. Neklyudov, and S. Bakai acknowledge the support of the Ukraine State Program “Nano-Technologies and Nano-Materials” through Project # 1.1.1.48.

### References

- [1] A.S. Bakai, Structure and Radiation Damage of Metallic Glasses, Progress in Physics of Metals 3 No. 1, 2002, 87–106.
- [2] Yu. Petrusenko, A. Bakai, V. Borysenko, D. Barankov, O. Astakhov, M.-P. Macht, Mater. Res. Soc. Symp. Proc. 1048 (2008) Z05–13.
- [3] Yu. Petrusenko, A. Bakai, I. Neklyudov, V. Borysenko, D. Barankov, O. Astakhov, M.-P. Macht, Problems of Atomic Science and Technol., Series: Physics of Radiat. Effect and Radiat. Mater. Science No. 2, 2008, 62–65.
- [4] D. Qiao, G. Wang, W. Jiang, Y. Yokoyama, P.K. Liaw, H. Choo, Mater. Trans. 48 (7) (2007) 1828–1833.
- [5] A.S. Bakai, I.M. Mikhailovskij, T.I. Mazilova, Low Temp. Phys. 28 (2002) 279.
- [6] A.S. Bakai, S.A. Bakai, G.N. Malik, V.M. Gorbatenko, V.M. Netesov, V.A. Emlyaninov, Problems of Atomic Science and Technology Series: Physics of Radiat. Effect and Radiat. Mater. Science No. 4, 2005, 104–107.
- [7] A.S. Bakai, Polycluster Amorphous Solids, Energoatomizdat, Moscow, 1987 (in Russian).
- [8] A.S. Bakai, in: H. Beck, H.-J. Guntherodt (Eds.), Glassy Metals III, Springer, Heidelberg, 1994, pp. 209–252.
- [9] V. Borysenko, Y. Petrusenko, D. Barankov, Mater. Res. Soc. Proc. 1215 (2010), 1215-V17-04.
- [10] Z.F. Zhang, J. Eckert, L. Schultz, J. Mater. Res. 18 (2003) 456.
- [11] I.M. Mikhailovskij, G.D.W. Smith, N. Wanderka, T.I. Mazilova, Ultramicroscopy 95 (2003) 157.
- [12] T. Egami, S.J. Poon, Z. Zhang, V. Keppens, Phys. Rev. B 76 (2007) 024203.
- [13] Zh. Zhou, C. Uher, D. Xu, W.L. Johnson, W. Gannon, M.C. Aronson, Appl. Phys. Lett. 89 (2006) 031924.